Measurement of mean wear coefficient during gear tests under various operating conditions

José A. Brandão, Pedro Cerqueira, Jorge H.O. Seabra, Manuel J.D. Castro

A B S T R A C T

Seven wear tests were conducted on an FZG gear testing machine in order to ascertain the influence of basestock (PAO and mineral), specific film thickness and contact load on the wear of spur gears, particularly on the wear coefficient κ that is used in Archard's law. The results showed that load may have some influence on the wear coefficient. They also showed that the influence of specific film thickness on wear is very non-linear. The influence of basestock, even with oils of similar viscosity, is very significant, as much as any other parameter in isolation.

Keywords:

Gear
Wear
Micropitting

1. Introduction

Wear, the process by which material is removed from a surface that rubs against another, has always been of interest for tribologists. However, the focus in the study of wear has tended to be on occurrences of excessive wear, not on mild wear. In particular, mild wear in lubricated gears has been largely neglected as an object of study. This state of affairs changed in the 1990s, when authors directed their attention to this phenomenon.

Many of the new studies were concerned with the application of a model of mild wear in gears. Most models are based on variants of the Archard wear law [1]:

$$dh = kp|\Delta u|\,dt \tag{1}$$

presented here in a localised form, where h is the wear depth, t is the time, p is the normal pressure, Δu is the sliding velocity and k is the wear coefficient given typically in [Pa^{-1}]. The wear coefficient k is a property of the interface, depending on the contacting materials, operating conditions, tooth flank surface roughness, and on the lubricant, in case of lubricated contacts.

Flodin and Anderson created one such model that they then applied to the prediction of wear to spur and helical gears [2–4].

The research group gathered around Ahmet Kahraman at Ohio State University developed a surface wear prediction methodology that they applied to spur and helical gears [5], including effects of profile deviations, manufacturing errors, profile modifications [6] and the interaction of wear with dynamic loads [7].

This last aspect, the interaction of wear and dynamic loads, has been intensely studied [8–11] with the conclusion that wear can alter significantly the frequencies and peaks of dynamic loads.

Brauer and Andersson [12] conducted a theoretical study of wear in spur gears with interference, using a mixed finite element (FE) and analytical approach. Their results showed that wear of gear tooth flanks may eliminate interference.

Park et al. [13] proposed a method for the computation of the surface wear of hypoid gear pairs, combining Archard's wear model with a semi-analytical hypoid gear contact model.

The brief enumeration of publications above shows the abundance of theoretical studies of mild wear in lubricated gears. Surprisingly, no such wealth of experimental work on gear mild wear is to be found. This is surprising because it is generally acknowledged that the wear coefficient k can only be obtained from direct measurement, that it is very dependent on the contact conditions and materials and that it is imprudent to extrapolate results of one set of measurements to different operating conditions.

Flodin [14] conducted a wear test on an FZG gear testing machine. The tested gears were an FZG type C-PT gear pair, loaded to load stage 10 (corresponding to 1539 MPa Hertzian stress at pitch point), with a pinion rotational speed of 100 RPM, lubricated with an ISO VG 68 unadditised mineral oil at 90 °C of temperature.

To study wear on gears experimentally, Krantz and Kahraman [15] used results from prior tests on gears performed by Townsend and Shimski [16] for other purposes. These tests were conducted

on a closed-power-loop gear testing machine in which the load is applied by an hydraulic cylinder. The tests were 7 in number; and each test consisted in applying the same operating conditions on identical gears while varying only the lubricating oil: each oil was formulated from the same mineral basestock, but had different viscosities from each other (viscosities ranged from 12.2 to 52.4 cSt at 40 °C). The analysis of wear on the gears showed that wear increases as the specific film thickness Λ decreases ($\Lambda = h_0/R_q$, where h_0 is the central film thickness and R_q is the combined RMS roughness of the contacting surfaces). This is roughly in line with the law proposed by Priest and Taylor [17], which relates the wear coefficient in piston rings to the lubrication regime through a dependence of k on the specific film thickness.

İmrek and Düzcükoğlu [18] sought to isolate the effect of pressure on wear by comparing two experiments performed on an FZG machine: one with gears of uniform width and the other with gears of variable width, chosen to keep the Hertzian pressure approximately constant along the line of action, which entails a sudden change in width in the single tooth pair contact area. In this case also, one single set of operating conditions was used.

It can be seen that no attempt has so far been made to obtain wear coefficients when gears are operated under diverse sets of operating conditions. The present work attempts to "plug this hole": gear tests on the FZG machine were performed under different operating conditions. The parameters selected for study were the specific film thickness Λ, which has elsewhere already been identified as a key influence on the wear coefficient k, the basestock of the lubricant and the contact load between the gears.

The wear coefficient to be measured is the main parameter to be used in a wear simulation model [19] so that it can be included in another model of concurrent wear and contact fatigue model [20].

2. Experimental procedure

The tests were conducted on a back-to-back spur gear test rig with power recirculation: the well known FZG gear test rig [21]. The tested gears were FZG type C-CF spur gears [22], whose main properties can be found in Table 1.

The gears were dip lubricated with two fully additised ISO VG 150 commercial gear oils, one highly refined mineral gear oil (MIN) and one poly-alphaolefin synthetic gear oil (PAO), depending on the test. This is intended to ascertain the influence of the basestock on wear, in particular on the wear coefficient.

Some properties of the oils are listed in Table 2. The properties in the first 6 rows (from density to flashpoint) were extracted from the oil suppliers' information sheets. The remaining properties were obtained from other sources.

Table 1
Properties of the FZG C-CF gears.

Property	**Pinion**(**1**)	**Wheel** (**2**)
Material	16MnCr5	
Treatment	case-carburised	
Surface hardness	750 HV1	
DIN3962 grade	5	
Tip relief	no	
Root relief	no	
Crowning	no	
Centre distance a (mm)	91.5	
Module m (mm)	4.5	
Pressure angle α (deg)	20	
Number of teeth Z	16	24
Tooth width b (mm)	14	14
Profile shift x	0.1817	0.1715
Addendum diameter d_a (mm)	82.46	118.36
Roughness Ra (μm)	0.5	0.5
Combined RMS roughness σ (μm)	0.79	

Table 2
Oil properties.

Property	PAO	MIN
Density at 15 °C ρ_{15} (kg/m^3)	849	890
Kinematic viscosity at 40 °C ν_{40} (cSt)	150	150
Kinematic viscosity at 100 °C ν_{100} (cSt)	19.4	14.5
Viscosity index VI	148	>95
Pour point (°C)	<-57	-18
Flash point (°C)	250	220
Reference temperature T_{ref} (°C)	40	40
Reference viscosity η_{ref} (mPa s)	127	130.8
Thermal-viscous index S_0 (–)	1.093	1.271
Piezo-viscous index Z (–)	0.467	0.608
Lubricant parameter $\alpha\eta$ at 80 °C (ns)	0.3231	0.3538
Lubricant parameter $\alpha\eta$ at 90 °C (ns)	0.2290	0.2400
Lubricant parameter $\alpha\eta$ at 100 °C (ns)	0.1670	0.1685
Thermal conductivity K_f (W m^{-1} K^{-1})	0.154	0.137

The variation of viscosity with pressure and temperature is presumed to follow Roelands' equation [23]:

$$\ln\frac{\eta}{\eta_{ref}} = (\ln\eta_{ref} + 9.67)\cdot\left\{\left(\frac{T-138}{T_{ref}-138}\right)^{-S_0}\cdot\left(1+\frac{p}{0.196}\right)^{Z}-1\right\} \quad (2)$$

where Z and S_0 are dimensionless parameters of the oil, T_{ref} is a reference temperature in K, η_{ref} is the dynamic viscosity at the reference temperature and atmospheric pressure in Pa · s, T is the temperature of the lubricant in K, p is the pressure in GPa and η is the low shear dynamic viscosity in Pa · s. The parameters of the oils were estimated following the method presented by Brandão et al. [24] and are included in Table 2.

There are a number of competing definitions of the piezo-viscosity coefficient to be used for film thickness calculation, this is in fact a subject of contention among researchers. The simplest definition is used here, in line with Gold et al. [25], the tangent piezo-viscosity coefficient at 0.2 GPa: $\alpha_{0.2} = \ln(\eta/\eta_0)/(0.2\ \text{GPa})$. The lubricant parameter $\alpha\eta$, which figures in film thickness calculation formulas, is also given in Table 2 at relevant temperatures.

Larsson and Andersson [26] measured the thermal conductivity of mineral and PAO oils. Their results were used here and are listed in Table 2.

Inductively Coupled Plasma (ICP) mass spectrometry was performed on the oils, and the results are shown in Table 3. Although the precise formulation of the commercial oils is not available, the presence of chemical elements is a clue as to the type of additives in each oil. In the case of PAO, detection of phosphorus, sulphur and boron indicates the possible presence of anti-wear and extreme pressure additives; and detection of calcium indicates the presence of detergent additives. In the case of MIN, detection of phosphorus and zinc indicates the presence anti-wear and extreme pressure additives; and detection of calcium, barium and magnesium indicates the presence of detergent additives.

Table 3
ICP oil analysis result.

Element	PAO	MIN
P (ppm)	210	280–380
S (ppm)	4630	N/A
B (ppm)	<30	N/A
Ca (ppm)	13	4
Ba (ppm)	0	4
Mg (ppm)	0	4
Zn (ppm)	0	4
Si, Pb, Li, Al, Cd, Cr, Cu, Fe, K , Mn, Mo, Na, Ni, Sn, Ti, V (ppm)	0	N/A

Table 4
Operating conditions of each test.

ID	T01	T11	T12	T02	T03	T03b	T04
Oil	PAO	PAO	PAO	PAO	PAO	PAO	MIN
Oil temperature T_0 (°C)	100	100	100	80	90	90	100
Pinion velocity n_1 (rpm)	750	750	750	4500	2550	2550	750
Load stage	K9	K7	K5	K9	K9	K9	K9
Contact load F_N (N)	6373	3917	2069	6373	6373	6373	6373
Avg. spec. film thick. $\overline{\Lambda}$	0.12	0.12	0.12	0.46	0.30	0.30	0.12
Pitch spec. film thick. Λ_C	0.12	0.12	0.13	0.65	0.36	0.36	0.12
Pitch $p_{0,C}$ (MPa)	1408	1104	802.3	1408	1408	1408	1408
Pitch half-width a_C (μm)	205.2	160.9	116.9	205.2	205.2	205.2	205.2

Seven tests were performed in total. The duration of each test was selected to ensure that the pinion completed 5.4 million revolutions. The operating conditions of each test are listed in Table 4, in which each columns from 2 to 8 shows the operating conditions of a particular test. As an example, column 2 shows the operating conditions under which test T01 was run: lubrication by the PAO oil, oil sump temperature of 100 °C, 750 RPM pinion rotational speed, load stage K9. This leads to a contact load F_N=6373 N, a mean specific central film thickness of $\overline{\Lambda}=0.12$, a specific central film thickness at pitch point $\Lambda_C=0.12$, a maximum Hertzian pressure at pitch point $p_{0,C}=1408$ MPa, a contact half-width at pitch point a_C=205.2 μm.

Test T01 is used as the reference test, from which all other diverge in a single parameter. Tests T11 and T12 are performed to show the influence of load on wear. Tests T02 and T03 are intended to show the influence of specific film thickness on wear, notice that the variation in film thickness is obtained through a change in both angular velocity of the gears and temperature of the oil. This was done to get a wider variation of specific film thickness than would have been possible by changing only the angular velocity of the gears, because the FZG machine on site only allows pinion rotational speeds up to 4500 rpm. Test T03b is a repetition of test T03 to evaluate the repeatability of the tests. Test T04 is intended to show the influence of the oil basestock on wear.

The specific central film thickness was computed, not measured. The Grubin formula, given by Dowson and Higginson [27], was used to compute the uncorrected central film thickness:

$$h_0 = 1.95R^{0.364}\left[\alpha\eta_0(U_1+U_2)\right]^{0.727}\left(E'b/F_N\right)^{0.091} \tag{3}$$

where R is the effective radius of curvature, given by $R=\left(R_1^{-1}+R_2^{-1}\right)^{-1}$; E' is the effective Young modulus, given by $E'=2\left[(1-\nu_1^2)/E_1+(1-\nu_2^2)/E_2\right]^{-1}$; R_1 and R_2 are the radii of curvature of the pinion and wheel surface, ν_1 and E_1 are the poisson ratio and the Young modulus of the pinion, respectively; ν_2 and E_2 are the poisson ratio and the Young modulus of the wheel, respectively; η_0 is the viscosity of the lubricant in the inlet; α is the pressure-viscosity coefficient.

Several formulas exist for the calculation of the correction to film thickness due to shear heating: for example, Gupta et al. [28] presented such a formula. Here, however, this was computed from Gohar [29]:

$$\phi_T = \left\{1+0.1\left[1+14.8\left(\frac{|U_1-U_2|}{U_1+U_2}\right)^{0.83}\right]\left(\frac{\beta(U_1+U_2)\eta_0}{K_f}\right)^{0.64}\right\}^{-1} \tag{4}$$

where ϕ_T is the inlet shear heating correction factor, β is the thermoviscosity coefficient and K_f is the thermal conductivity of the lubricant.

The correction for inlet shear-thinning was also applied, as recommended by Bair and Winer [30]:

$$\phi_{NN} = \left[1+4.44\left(\frac{\eta_0(U_1+U_2)/2}{h_0G}\right)^{1.69}\right]^{1.26(1-n)^{1.79}} \tag{5}$$

where G (Pa) and n are the parameters of the Carreau equation for shear thinning. Bair [31] lists these parameters for a different set of lubricating liquids. The values for G and n used here were those of the liquids in [31] most similar to PAO and MIN: for PAO, G=1.4 GPa and n=0.625 and for MIN, G=3.4 GPa and n=0.65.

The specific central film thickness corrected for inlet shear heating is then:

$$\Lambda = \frac{(\phi_T/\phi_{NN})h_0}{\sigma} \tag{6}$$

The sequence of operations to perform each test was as follows:

1. Choose a pair of untested gears.
2. Clean the gears in ultrasonic bath of petroleum ether.
3. Weigh the pinion. The weighting precision is approximately ± 1 mg.
4. Take roughness measurements (topographies) on the flank surfaces of teeth 1 and 9 of the pinion and of teeth 1, 9 and 17 of the wheel.
5. Clean the FZG test gearbox with petroleum ether and mount the gears in the gearbox, adding 1 l of lubricating oil for dip lubrication.
6. Set the operating conditions in the FZG controlling unit and run the test for 5.4 million revolutions of the pinion (3.6 million revolutions of the wheel).
7. Immediately upon completion of the test, take an oil sample to be analysed.
8. Clean the gears as before.
9. Weigh the pinion.
10. Repeat the roughness measurements on the same tooth flanks.

Notice that there was no running-in stage: each test was performed under the same operating conditions from beginning to end.

3. Evaluation of the mean wear coefficient from the measured mass loss

Archard [1] published in 1953 his famous wear law, which describes the wear volume loss due to the sliding contact between flat surfaces:

$$\frac{\Delta V}{S} = \frac{K}{H}F_N \tag{7}$$

where ΔV is the volume loss, S the sliding distance, K the dimensionless wear coefficient, H the softer surface's hardness and F_N the normal contact load.

To use Archard's wear law in the more complex case of contact between gear teeth, it must be written in a differential form:

$$\frac{dh(x,t)}{dt} = \kappa p(x,t)\,|U_2(t)-U_1(t)| \tag{8}$$

where h is the wear depth, p the contact pressure and κ the wear coefficient (with units of Pa^{-1}). The coordinate x is the position on the surface of the tooth shown in Fig. 1 and t is the time coordinate. U_2 and U_1 are the tangential velocities of the contacting surfaces.

Generally, one can suppose that the wear coefficient will change as the conditions of lubrication change. However, one can obtain the mean wear coefficient $\overline{\kappa}$ by remembering that the mean

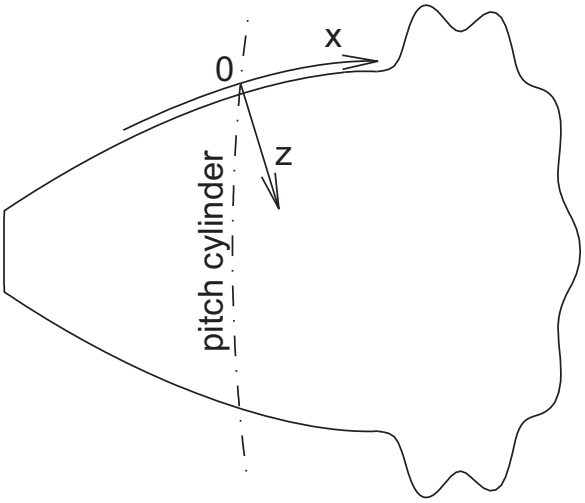

Fig. 1. Coordinates on the surface of the pinion tooth flank.

wear coefficient is a hypothetical constant wear coefficient that would lead to the same volume loss found in reality. Hence, the mean wear coefficient can be used in all calculations as a constant, even though the true, non-averaged wear coefficient may vary in time.

During one full revolution of the pinion, a point situated at coordinate x on one of its teeth will then have its height diminished by:

$$\delta h(x) = \int_{t_A}^{t_E} \overline{\kappa} p(x,t) |\, U_2(t) - U_1(t) \,| \, dt \tag{9}$$

where t_A is the instant when the tooth first comes in contact with its counterpart on the wheel and t_E is the instant when the tooth ceases contact.

On the same tooth, the volume lost to wear during one single revolution will then be:

$$\delta V = \int_{x_E}^{x_A} \delta h(x) b dx = \int_{x_E}^{x_A} \int_{t_A}^{t_E} b \overline{\kappa} p(x,t) |\, U_2(t) - U_1(t) \,| \, dt dx \tag{10}$$

Or:

$$\delta V = \int_{t_A}^{t_E} \left[\int_{x_E}^{x_A} p(x,t) b dx \right] \overline{\kappa} |\, U_2(t) - U_1(t) \,| \, dt \tag{11}$$

And finally:

$$\delta V = \overline{\kappa} F_N \int_{t_A}^{t_E} \frac{F_{N,1}}{F_N} |\, U_2(t) - U_1(t) \,| \, dt \tag{12}$$

where $F_{N,1}$ is the share of contact load F_N on the specific tooth (F_N can be distributed among several pairs of contacting teeth). In consequence, the volume lost by all Z teeth during all N_{turns} revolutions of the gear is given by:

$$\Delta V = N_{\text{turns}} Z \delta V = \overline{\kappa} F_N \left[N_{\text{turns}} Z \int_{t_A}^{t_E} \frac{F_{N,1}}{F_N} |\, U_2(t) - U_1(t) \,| \, dt \right] \tag{13}$$

If one has access to the measured mass loss ΔM on a gear, the mean wear coefficient can be deduced. If one accepts that the density $\rho = 7850$ kg/m^3 of the gear steel remains constant during the tests, the volume loss ΔV is easily computed:

$$\Delta V = \Delta M / \rho \tag{14}$$

Hence the mean wear coefficient can be estimated from the expression:

$$\overline{\kappa} = \frac{\Delta M}{F_N N_{\text{turns}} \rho Z \int_{t_A}^{t_E} \frac{F_{N,1}}{F_N} |\, U_2(t) - U_1(t) \,| \, dt} \tag{15}$$

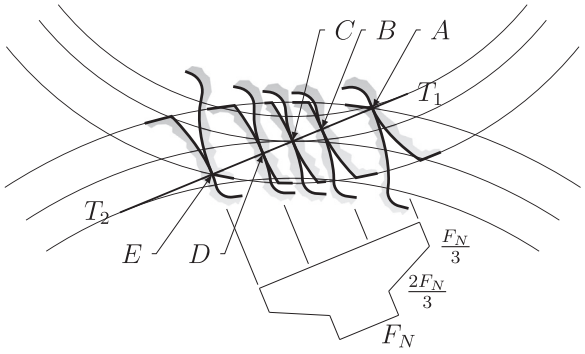

Fig. 2. Notable moments of the meshing of a pair of teeth: the consecutive positions of a pair of contacting teeth are shown superimposed, as well as the share of the normal load borne by this pair of teeth as a function of the contact position along the contact line.

The denominator on the right-hand side of the expression can be computed analytically so long as the evolution of the contact load on a specific tooth pair is known along the line of action.

For the present, specific case of an FZG-CF pinion gear, dynamic effects on the contact load between gears were disregarded and in evaluating the share of the contact load on a particular pair of gears at any particular instant during gear meshing, AGMA's recommendation [32] for gears with no root and tip relief was followed. This is illustrated in Fig. 2, where the following events are depicted:

- At instant t_A, the pair of teeth first comes into contact at point A and the normal contact load is $F_{N,1} = F_N/3$.
- Between instants t_A and t_B, the contact load increases linearly.
- At instant t_B, a previous tooth pair disengages and the contact load jumps from $F_{N,1} = 2F_N/3$ to $F_{N,1} = F_N$.
- At instant t_C, the theoretical tooth pair contact is on the pitch point at C.
- At instant t_D, another tooth pair comes into contact at D and the contact load drops from $F_{N,1} = F_N$ to $F_{N,1} = 2F_N/3$.
- Between instants t_A and t_B, the contact load decreases linearly.
- At instant t_E, the tooth pair disengages at E, and the normal contact load is $F_{N,1} = F_N/3$.

In this case, where the aim is to determine the mean wear coefficient from the mass loss on the pinion, the following integral can be calculated and will be the same under any set of operating conditions (for the pinion):

$$\int_{t_A}^{t_E} \frac{F_{N,1}}{F_N} |\, U_2(t) - U_1(t) \,| \, dt = 2.535 \text{ mm} \tag{16}$$

Consequently, considering the properties of the pinion:

$$\overline{\kappa} = 3.140 \times 10^{-3} \frac{\Delta M}{N_{\text{turns}} F_N} \tag{17}$$

where ΔM must be in (kg), F_N in (N) and the result comes out in (Pa^{-1}).

4. Experimental results and discussion

4.1. Mass loss and wear coefficient

Fig. 3 gives the mass loss results – ΔM (mg) – obtained by computing the difference between weighings of the pinion before and after a test. The graph is organised into four subfigures, all with the same scale: Fig. 3a deals with the variation of mass loss with load; Fig. 3b, with mean specific thickness; Fig. 3c, with

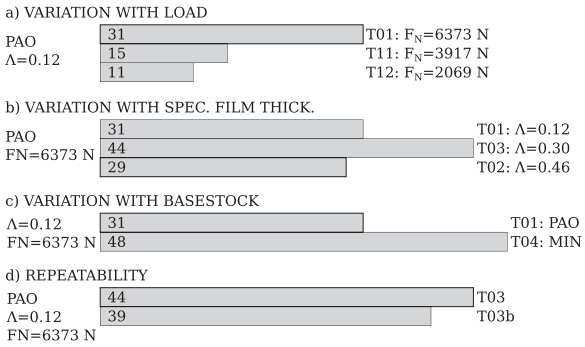

Fig. 3. Measurements of mass loss ΔM (mg) on the pinion.

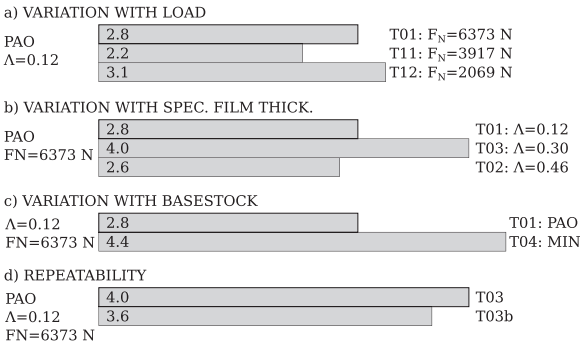

Fig. 4. Mean wear coefficient $\overline{\kappa}$ (10^{-18} Pa^{-1}).

basestock; and Fig. 3d shows two tests run with the same parameters.

The way in which Fig. 3a shows the variation of mass loss with load is by displaying one above the other horizontal bars that give the measurement for each of tests T01, T11 and T12, shown in order of decreasing contact load. To the left of the bars are printed the conditions of operation that were kept the same in all three tests. To the right of the bars are shown the test code and value of the operating condition that is changed. Fig. 3a gives the completely unsurprising result that mass loss increases with load.

Fig. 3b is organised similarly to Fig. 3a. Notice how test T01, the base case, is shown again, for comparison. It would be expected that mass loss would decrease with increasing specific film thickness, but that is not the story told by the figure: it is true that there is a decrease in mass loss when going from $\overline{\Lambda} = 0.30$ to $\overline{\Lambda} = 0.46$, but the opposite is true when going from $\overline{\Lambda} = 0.12$ to $\overline{\Lambda} = 0.30$. The answer to this puzzle must be found in the fact that the tests were performed with oils at different temperatures: 100 °C for test T01, 90 °C for T03 and 80 °C for T02. This was done to get a wider variation of specific film thickness than would have been possible by changing only the angular velocity of the gears. Since the (at first glance) incongruously low mass loss occurs with the test with very low $\overline{\Lambda}$ and high temperature, this may be a case of thermal activation of additives. The assumption that film thickness is the only lubrication parameter to consider for wear is thus shown to be false: temperature should be considered as well.

Fig. 3c, organised similarly to Fig. 3a, shows that changing from a synthetic PAO to a mineral oil of similar viscosity gives rise to a greater increase in mass loss than can be obtained with a change in load or a change in specific film thickness alone. Once more, this is not a surprising or new result. However, the magnitude of variation can be compared here with the influence of load and film thickness for gears.

Finally, Fig. 3c gives the mass loss for two tests (T03 and T03b) that were run with the same parameters. It can be seen that, between tests that in theory should give the same result, the mass loss can differ by 5 mg. This gives an estimate of what constitutes a non-significant difference. This is still lower than the variations observed in Fig. 3a–c, so they must be significant.

Using the method detailed in Section 3, the mean wear coefficient $\overline{\kappa}$ was estimated from each measurement of mass loss and Fig. 4 was constructed. It is organised similarly to Fig. 3.

Fig. 4 d shows that repetition of a test can give differences of 0.4×10^{-18} Pa^{-1} in wear coefficient. This is therefore an estimate of the precision in measurement that can be achieved with the current experimental setup.

It is generally assumed that the wear coefficient is independent of the contact load. However, Fig. 4a, which shows the variation of $\overline{\kappa}$ with load, is inconclusive in that respect. While tests T01 and T12 give essentially the same wear coefficient $2.8 - 3.1 \times 10^{-18}$ Pa^{-1}, test T11 gives a lower wear coefficient (2.2×10^{-18} Pa^{-1}). The difference is slightly larger than the difference in Fig. 4d, which might or might not mean that it is significant.

Figs. 4b and c give rise to the same comments that were made about Figs. 3b and c, respectively.

Observing the subfigures together, it is clearly the case that the variation of the wear coefficient with load is much smaller than that with specific film thickness or with basestock (which are roughly the same).

4.2. Direct reading ferrography

A small volume (1 ml) of each lubricant sample taken after the tests, diluted with a dilution factor $d = 0.1$, was submitted to Direct Reading Ferrography examination. The results in terms of large particle count (D_L) and small particle count (D_S) is shown in Fig. 5. The figure is organised similar to Fig. 3: it constituted of four subfigures, each dealing with the variation with regard to one single parameter, which are plotted as grey horizontal bars. On the left side of the bars are found the parameters that share the same value among tests, on the right side is found the parameter that changes from test to test.

Study of Fig. 5 shows the same tendencies as Fig. 3, both for D_L and for D_S. There is, however, a big difference found in Fig. 5b: the large increase in wear particle count when increasing the specific film thickness from 0.12 to 0.3 and 0.46. This is especially odd because the mass loss in tests T01 and T02 is roughly the same, while particle counts are very different. This seems to give credence to the idea that a different wear regime is in action under the lowest $\overline{\Lambda}$ (which corresponds to the hottest temperature). A difference in behaviour between the PAO and MIN oils can also be observed in Fig. 5c: the large increase in wear, upon switching from PAO to MIN, is mirrored by an increase in the large particle count D_L; however, the small particle count D_S decreases instead. Hence, larger particles are produced with MIN than with PAO. This is confirmed in Figs. 8a and d, showing micrographs of particles produced in each case.

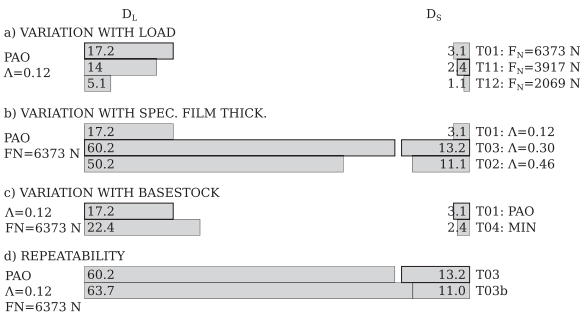

Fig. 5. Direct reading ferrography: large particles (D_L) and small particles (D_S).

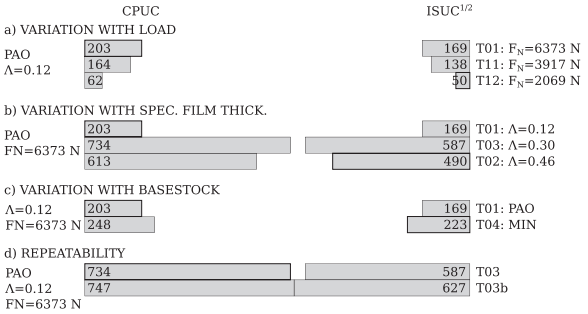

Fig. 6. Direct reading ferrography: wear particles concentration (*CPUC*) and wear severity index (*ISUC*).

From the particle count D_L and D_S can be computed the wear particle concentration $CPUC = (D_L + D_S)/d$ and the wear severity index $ISUC = (D_L^2 - D_S^2)/d^2$. Fig. 6 was constructed with the results. It is organised exactly like Fig. 5. However, instead of showing *ISUC*, it shows $\sqrt{ISUC}$ because it is in a more convenient scale for representation. Fig. 6 confirms the observations made in Fig. 5.

4.3. Analytical ferrography

Fig. 7 shows the core of the ferrograms of tests T01, T11, T02 and T04. Comparing Fig. 7a (T01) with Fig. 7b gives an indication of the influence of load on wear particles: the photographs are similar but the ferrogram of T01 is more densely populated.

Comparing Fig. 7a (T01) with Fig. 7c gives an indication of the influence of film thickness on wear particles. Clearly, the ferrograms are different and the ferrogram corresponding to test T02 is much denser.

Comparing Fig. 7a (T01) with Fig. 7d gives an indication of the influence of oil basestock on wear particles. The ferrograms are radically different, test T04 leads to many more particles, all clumped together, instead of being spread out as is the case for tests T01, T11 and T02.

All of this is in accordance with the mass loss and wear index results.

In Fig. 8, details of wear particles are shown for tests T01, T11, T02 and T04. Fig. 8a shows a micropitting particle, indicating that this mode of damage is present in test T01.

Fig. 8b is an indication that fatigue also occurred during test T11, further showing the similarity between test T01 and T11 in terms of wear. In other parts of the ferrogram of test T11, combined fatigue and wear particles can also be found.

Fig. 8c shows a very large wear particle that can even be made out in Fig. 7c, which suggests that severe wear is occurring during test T02. Elsewhere in the ferrogram, ferrous oxide particles and corrosion particles can be found. This is very different from the particles encountered in the ferrogram of test T01, which further outlines the change in wear regime that takes place with the increase in specific film thickness from the lowest level.

Fig. 8d shows that a great number of big fatigue and combined fatigue and wear particles were formed during test T04.

4.4. Roughness

Fig. 9 shows roughness profiles extracted from topographies of pinions, filtered with a Gaussian filter (cut-off 0.8 mm). The figure is organised into four subfigures. As an example, Fig. 9a shows two profiles that were extracted from topographies of a tooth flank on a pinion that had been subjected to test T01: one profile labelled as 'unworn', meaning that the measurement was taken before having applied the test, and the other profile marked as 'worn', meaning

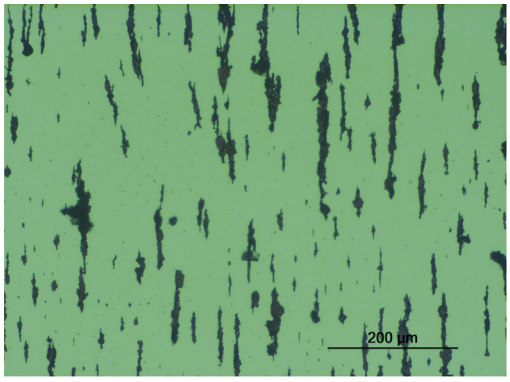

a) T01: PAO, $\overline{\Lambda} = 0.12$, $F_N = 6073$ N, $CPUC = 203$

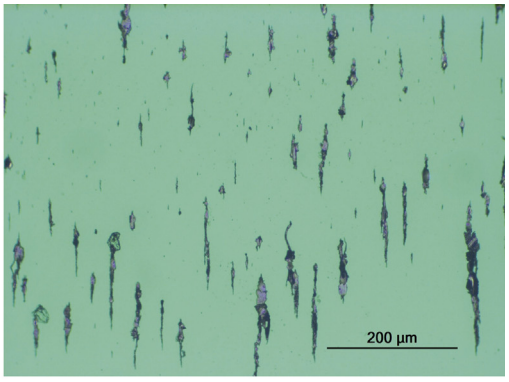

b) T11: PAO, $\overline{\Lambda} = 0.12$, $F_N = 3917$ N, $CPUC = 164$

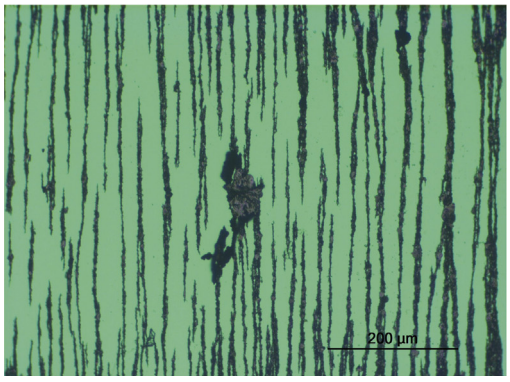

c) T02: PAO, $\overline{\Lambda} = 0.46$, $F_N = 6073$ N, $CPUC = 613$

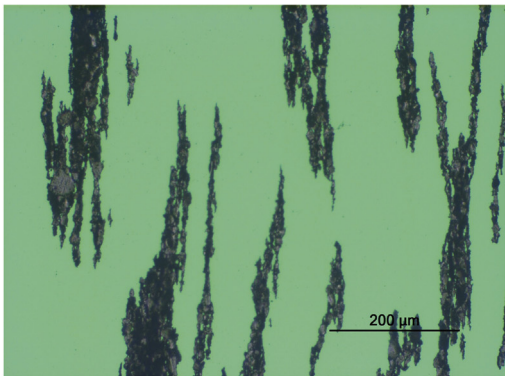

d) T04: MIN, $\overline{\Lambda} = 0.12$, $F_N = 6073$ N, $CPUC = 248$

Fig. 7. Analytical ferrography: view of the core for tests (a) T01, (b) T11, (c) T02, and (d) T04.

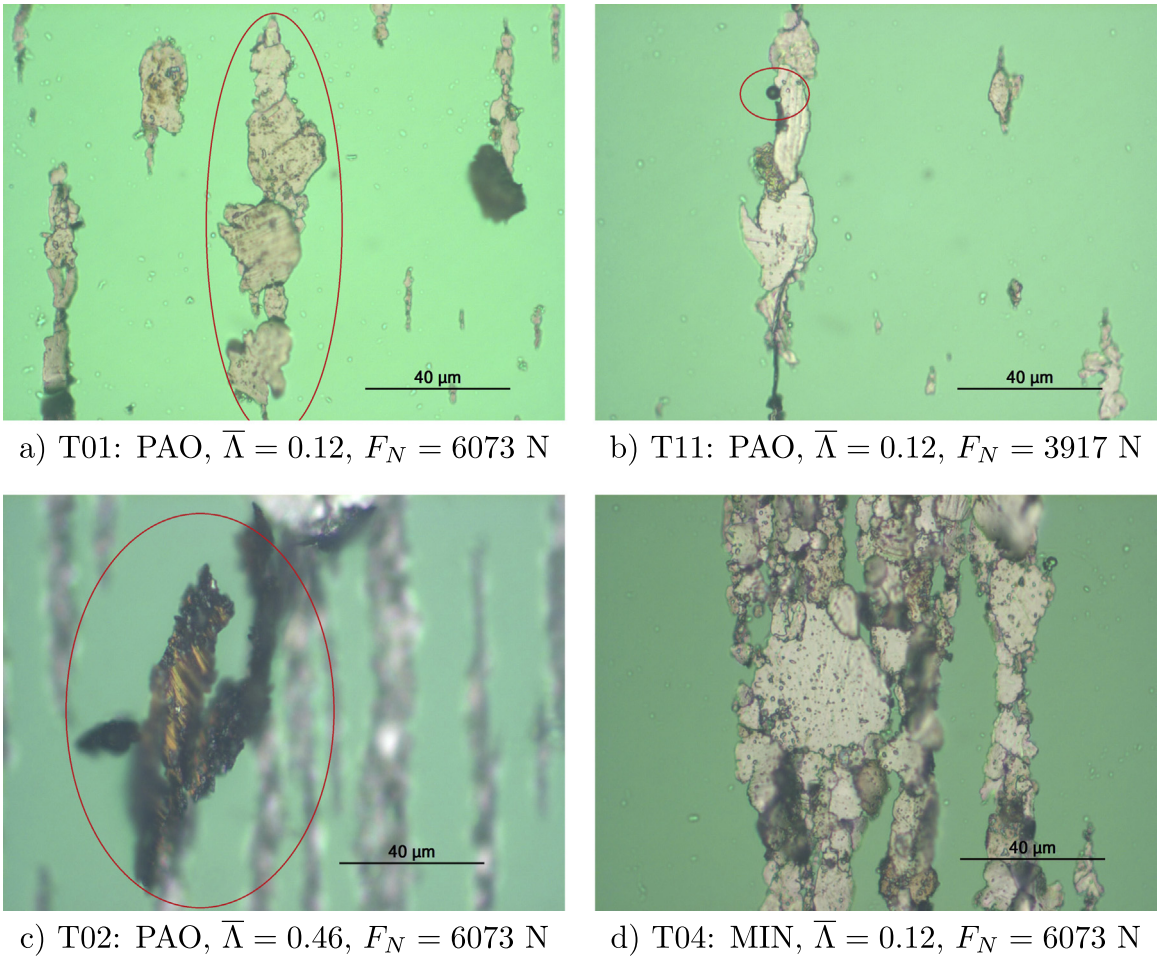

a) T01: PAO, $\overline{\Lambda} = 0.12$, $F_N = 6073$ N b) T11: PAO, $\overline{\Lambda} = 0.12$, $F_N = 3917$ N

c) T02: PAO, $\overline{\Lambda} = 0.46$, $F_N = 6073$ N d) T04: MIN, $\overline{\Lambda} = 0.12$, $F_N = 6073$ N

Fig. 8. Analytical ferrography: view of details of wear particles for tests (a) T01, (b) T11, (c) T02, and (d) T04.

that the measurement was taken after having applied the test. Extreme care was taken to extract, as much as possible, profiles located at the same position on the tooth flank. Notice a deep indentation near the tip of the tooth: this is an artificial mark added before the 'unworn' measurement to help in the correct localisation of the subsequent profile. The abscissa corresponds to the arc length on the surface of the tooth. Important points are marked as letters: point C is the pitch point; between point B and point D, the contact is between a single pair of teeth; outside this segment, contact is shared between two pairs of teeth.

The remaining subfigures, Figs. 9b,c and d, show the same information for tests T12, T03 and T04, respectively.

Comparison of the two profiles in Fig. 9a (test T01) shows that the variation of the roughness profile during test T01 is fairly modest, although micropits are noticeable below the pitch point. In general, the roughness is attenuated after the test.

In Fig. 9b (test T12, lower load), the evolution of roughness follows a similar pattern as in Fig. 9a, although only few micropits are visible below the pitch point.

Fig. 9c (test T03) shows a very different evolution from that in Fig. 9a. The roughness profile is very altered and large micropits have appeared above the pitch point. This is in keeping with the results previously presented, particularly the mass loss results.

Fig. 9 d (test T04) shows that a very deep alteration of the profile has taken place. In particular, the artificial groove at the tip seems to have been almost worn away and many crags and valleys have appeared below the pitch point. Once more, this is in keeping with the mass loss results, or indeed all other results previously shown.

It would be interesting at this point to list some roughness parameters of the profiles shown in Fig. 9. However, it would be misleading to show the roughness parameter for the full length of a profile because the artificial marks are so large that they alter the roughness parameters. That is why only the length of profiles corresponding to $x < 5$ mm are used to compute the roughness R_a and RMS roughness R_q shown in Table 5.

Table 5 is instructive because it shows that the only test during which roughness increases is test T04, the one where the most wear occurred. Even during test T03, which saw significant wear and alteration of the profile, roughness decreased. This shows that roughness parameters are poor indicators of wear damage. This is in large part because no running-in stage was applied before the tests. The running-in effect of smoothing roughness still dominates the roughness parameters in all but one test.

5. Conclusion

Seven wear tests were conducted on an FZG gear testing machine in order to ascertain the influence of basestock, specific film thickness and contact load on wear of spur gears, particularly on the wear coefficient κ that is used in Archard's law. It was shown that:

- The choice of basestock is particularly significant: lubrication with a mineral oil leads to much higher wear than lubrication

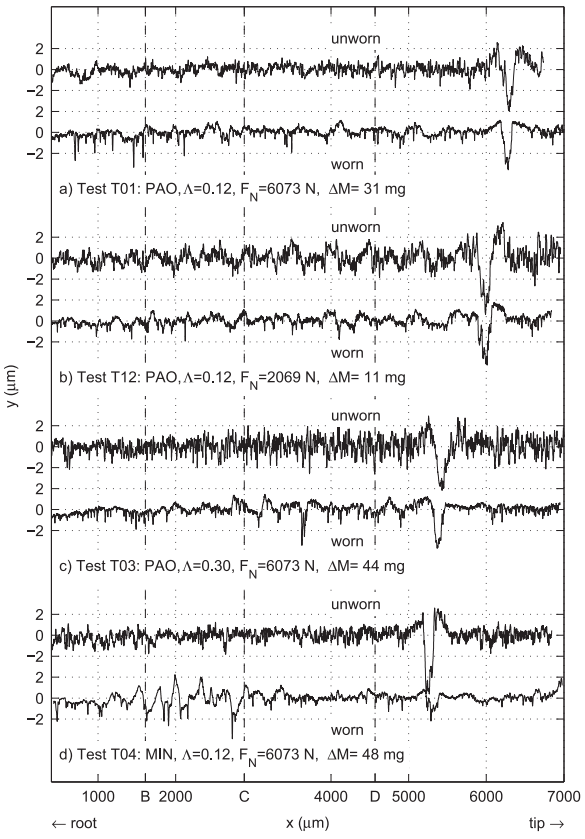

Fig. 9. Roughness profiles (both before and after gear testing) extracted from the topographies of pinion gear teeth that were submitted to test (a) T01, (b) T11, (c) T02, and (d) T04.

Table 5
Roughness parameters.

Test	T01	T12	T03	T04
R_a unworn (μm)	0.33	0.50	0.54	0.39
R_a worn (μm)	0.33	0.32	0.37	0.47
R_q unworn (μm)	0.42	0.63	0.69	0.49
R_q worn (μm)	0.45	0.41	0.49	0.64

with a PAO of similar viscosity. This was true for all wear parameters measured, including the wear coefficient.

- The influence of specific film thickness is unclear. At very low film thickness ($\overline{\Lambda} = 0.12$, boundary lubrication conditions) the wear behaviour was non-linear: wear was much lower than with much higher film thickness ($\overline{\Lambda} > 0.3$). This is very counter-intuitive, since one would expect that a higher frequency of direct collisions between asperities would lead to much higher wear. This may be because the lower film thickness was obtained in part by increasing temperature, thus potentially thermally activating the additives. If this is the case, one needs to revise the idea that the film thickness is the only lubrication parameter that influences wear coefficient (as implied by the law proposed by [17]): temperature might be an important factor.
- The influence of load is also unclear. It is certain that an increase in load also increases wear: this was amply shown in all measurements. However, Archard's law presupposes that the wear coefficient is largely independent of contact force. This was not entirely borne out by the experimental results, which show a dip in wear coefficient at an intermediate contact load. This dip seems to be deep enough to be significant.

From the above, it is clear that further testing is needed, in particular to separate the influence of specific film thickness from that of temperature.

Acknowledgements

The present work is funded by the European Regional Development Fund (ERDF) through the 'COMPETE – Competitive Factors Operational Program' and by Portuguese Government Funds through 'FCT – Fundação para a Ciência e Tecnologia' as part of:

- project 'High efficiency gears and lubricants for wind mill planetary gearboxes', reference number 'PTDC/EME-PME/100808/2008', for the experimental work;
- project 'Projecto Estratégico – LA 22 – 2011–2012', reference number 'Pest-OE/EME/LA0022/2011', for the rolling contact fatigue simulation;
- project 'Gear transmissions of high tribological efficiency and reliability', reference number 'EXCL/EMS-PRO/0103/2012', for the wear simulation.

References

[1] Archard J. Contact and rubbing of flat surfaces. J Appl Phys 1953;24(8):981–8.
[2] Flodin A, Andersson S. Simulation of mild wear in spur gears. Wear 1997;207(1):16–23.
[3] Flodin A, Andersson S. Simulation of mild wear in helical gears. Wear 2000;241(2):123–8. http://dx.doi.org/10.1016/S0043-1648(00)00384-7.
[4] Flodin A, Anderson S. A simplified model for wear prediction in helical gears, Wear 249 (3–4) (2001) 285–92. In: Proceedings of the ninth Nordic symposium on tribology. ⟨http://www.sciencedirect.com/science/article/pii/S0043164801005567⟩ http://dx.doi.org/http://dx.doi.org/10.1016/S0043-1648(01)00556-7.
[5] Bajpai P, Kahraman A, Anderson NE. A surface wear prediction methodology for parallel-axis gear pairs. J Tribol 2004;126(3):597–605. http://dx.doi.org/10.1115/1.1691433.
[6] Kahraman A, Bajpai P, Anderson NE. Influence of tooth profile deviations on helical gear wear. J Mech Des 2005;127(4):656–63. http://dx.doi.org/10.1115/1.1899688.
[7] Ding H, Kahraman A. Interactions between nonlinear spur gear dynamics and surface wear. J Sound Vib 2007;307(3–5):662–79. http://dx.doi.org/10.1016/j.jsv.2007.06.030.
[8] Kuang JH, Lin AD. The effect of tooth wear on the vibration spectrum of a spur gear pair. J Vib Acoust 2001;123(3):311–7. http://dx.doi.org/10.1115/1.1379371.
[9] Wojnarowski J, Onishchenko V. Tooth wear effects on spur gear dynamics. Mech Mach Theory 2003;38(2):161–78. http://dx.doi.org/10.1016/S0094-114X(02)00091-5.
[10] Onishchenko V. Tooth wear modeling and prognostication parameters of engagement of spur gear power transmissions. Mech Mach Theory 2008;43(12):1639–64. http://dx.doi.org/10.1016/j.mechmachtheory.2007.12.005.
[11] Osman T, Velex P. Static and dynamic simulations of mild abrasive wear in wide-faced solid spur and helical gears. Mech Mach Theory 2010;45(6):911–24. http://dx.doi.org/10.1016/j.mechmachtheory.2010.01.003.
[12] Brauer J, Andersson S. Simulation of wear in gears with flank interference–a mixed fe and analytical approach. Wear 2003;254(11):1216–32.
[13] Park D, Kolivand M, Kahraman A. Prediction of surface wear of hypoid gears using a semi-analytical contact model. Mech Mach Theory 2012;52:180–94. http://dx.doi.org/10.1016/j.mechmachtheory.2012.01.019.
[14] Flodin A. Wear investigation of spur gear teeth. Tribotest 2000;7(1):45–60. http://dx.doi.org/10.1002/tt.3020070106.
[15] Krantz T, Kahraman A. An experimental investigation of the influence of the lubricant viscosity and additives on gear wear. Tribol Trans 2004;47(1):138–48. http://dx.doi.org/10.1080/05698190490278949.
[16] Townsend DP, Shimski J. Evaluation of the EHL film thickness and extreme pressure additives on gear surface fatigue life. Technical report NASA-TM-106663. NASA Lewis Research Center, Cleveland, OH, United States; 1994. ⟨http://ntrs.nasa.gov/search.jsp?R=19940032811⟩.
[17] Priest M, Taylor C. Automobile engine tribology—approaching the surface. Wear 2000;241(2):193–203. http://dx.doi.org/10.1016/S0043-1648(00)00375-6 http://www.sciencedirect.com/science/article/pii/S0043164800003756.
[18] İmrek H, Düzcükoğlu H. Relation between wear and tooth width modification in spur gears. Wear 2007;262(3–4):390–4. http://dx.doi.org/10.1016/j.wear.2006.06.004.

[19] Brandão JA, Martins R, Seabra JHO, Castro MJ. Calculation of gear tooth flank surface wear during an FZG micropitting test. Wear 2014;311(1–2):31–9. http://dx.doi.org/10.1016/j.wear.2013.12.025.
[20] Brandão JA, Martins R, Seabra JH, Castro MJ. An approach to the simulation of concurrent gear micropitting and mild wear. Wear 2015;324–325:64–73. http://dx.doi.org/10.1016/j.wear.2014.12.001 http://www.sciencedirect.com/science/article/pii/S0043164814003706.
[21] Winter H, Michaelis K, FZG gear test rig – desciption and possibilities. In: Coordinate European council second international symposium on the performance evaluation of automotive fuels and lubricants; 1985.
[22] FVA. Test procedure for the investigation of the micro-pitting capacity of gear lubricants, FVA–information sheet 54/I-IV; 1993.
[23] Roelands CJA. Correlation aspect of viscosity–temperature–pressure relationships of lubricating oils [Ph.D. thesis]. Delft University of Technology; 1967.
[24] Brandão JA, Meheux M, Ville F, Seabra JH, Castro J. Comparative overview of five gear oils in mixed and boundary film lubrication. Tribol Int 2012;47:50–61. http://dx.doi.org/10.1016/j.triboint.2011.10.007.
[25] Gold PW, Schmidt A, Dicke H, Loos J, Assmann C. Viscosity–pressure–temperature behaviour of mineral and synthetic oils. J Synth Lubr 2001;18(1):51–79. http://dx.doi.org/10.1002/jsl.3000180105.
[26] Larsson R, Andersson O. Lubricant thermal conductivity and heat capacity under high pressure. Proc Inst Mech Eng Part J: J Eng Tribol 2000;214(4):337–42. http://dx.doi.org/10.1243/1350650001543223, URL ⟨http://pij.sagepub.com/content/214/4/337.abstract⟩.
[27] Dowson D, Higginson GR. Elasto-hydrodynamic lubrication, S.I. Edition. Oxford: Pergamon Press Ltd.; 1977.
[28] Gupta PK, Cheng HS, Zhu D, Forster NH, Schrand JB. Viscoelastic effects in MIL-L -7808-type lubricant, Part I: analytical formulation. Tribol Trans 1992;35(2):269–74. http://dx.doi.org/10.1080/10402009208982117.
[29] Gohar R. Elastohydrodynamics. Chichester: Ellis Horwood; 1988.
[30] Bair S, Winer WO. A simple formula for EHD film thickness of non-Newtonian liquids. In: Dowson D, Taylor CM, Childs THC, Dalmaz G, Berthier Y, Flamand L, Georges J-M, Lubrecht AA, editors. Elastohydrodynamics – 96, Fundamentals and applications in lubrication and traction. Proceedings of the 23rd Leeds-Lyon symposium on tribology held in the institute of tribology, Department of Mechanical Engineering, Tribology series, vol. 32. Elsevier; 1997. p. 235–41 ⟨http://www.sciencedirect.com/science/article/pii/S0167892208704528⟩ 10.1016/S0167-8922(08)70452-8.
[31] Bair S. The shear rheology of thin compressed liquid films. Proc Inst Mech Eng Part J: J Eng Tribol 2002;216(1):1–17 ⟨http://pij.sagepub.com/content/216/1/1.abstract⟩ 10.1243/1350650021543834.
[32] AGMA. Effect of lubrication on gear surface distress, AGMA information sheet, American Gear Manufacturers Association, 2003, 925-A03.